Optimization of Observer Trajectories for Bearings-Only Target Localization

YAAKOV OSHMAN, Senior Member, IEEE
PAVEL DAVIDSON
Technion–Israel Institute of Technology

The problem of bearings-only target localization is to estimate the location of a fixed target from a sequence of noisy bearing measurements. Although, in theory, this process is observable even without an observer maneuver, estimation performance (i.e., accuracy, stability and convergence rate) can be greatly enhanced by properly exploiting observer motion to increase observability. This work addresses the optimization of observer trajectories for bearings-only fixed-target localization. The approach presented herein is based on maximizing the determinant of the Fisher information matrix (FIM), subject to state constraints imposed on the observer trajectory (e.g., by the target defense system). Direct optimal control numerical schemes, including the recently introduced differential inclusion (DI) method, are used to solve the resulting optimal control problem. Computer simulations, utilizing the familiar Stansfield and maximum likelihood (ML) estimators, demonstrate the enhancement to target position estimability using the optimal observer trajectories.

Manuscript received March 6, 1977; revised October 22, 1997.

IEEE Log No. T-AES/35/3/06407.

This work was supported by the Department of Research and Development of the Israeli Ministry of Defense.

Authors' current address: Technion–Israel Institute of Technology, Dept. of Aerospace Engineering, Haifa 32000, Israel.

I. INTRODUCTION

Passive target localization using bearings-only measurements is a classical estimation problem, which has continued to be of great theoretical and practical interest since the pioneering work of Stansfield [1]. Basically, the problem is to estimate a fixed target position, based on a sequence of noisy bearing measurements, acquired by a (typically electro-optical) sensor which is mounted onboard a moving observer. The bearings are corrupted by a measurement noise, which is usually assumed to be Gaussian distributed. Bearings-only localization is especially important in situations where active measurements are either infeasible or prohibitive, such as military applications.

A vast amount of work has been performed in the area of bearings-only localization over the last five decades. In addition to Stansfield's estimator, one of the more popular approaches to the solution of this problem is the maximum likelihood (ML) approach [2]. Recursive algorithms, based on Kalman filtering techniques [3] or ML estimators [2], were applied for tracking moving targets using bearings-only measurements.

Although, in theory, target position can be estimated even without an observer maneuver, clearly such a maneuver can greatly enhance the estimator performance (i.e., accuracy, stability, and convergence rate). The inherent nonlinearity which characterizes the estimation problem makes the effect of the observer maneuver even more profound, rendering the observer maneuver an important factor which significantly affects the localization problem solution.

Several works have addressed the problem of determining optimal observer trajectories. In [4], the Cramer-Rao lower bound (CRLB) was used to examine the effect of course maneuvers on bearings-only target ranging. This study investigated the effects of course changes on estimation accuracy, but did not determine optimal observer trajectories. However, it did illustrate the importance of the observer maneuvers in this nonlinear estimation problem. Hammel, et al. [5] investigated the optimal observer trajectories problem in the context of continuous-time measurements (namely, assuming that the bearing measurements are acquired at an infinite rate). The performance index they used was based on the determinant of the Fisher information matrix (FIM). However, since that formulation rendered the resulting optimal control problem not suitable for standard solution methods (based on the minimum principle), Hammel, et al. proposed an approximate numerical solution, based on direct maximization of the determinant of the FIM for a finite number of course changes. In addition, they suggested an alternative performance index, based on a *lower bound* on detFIM. As shown later in this work, the suboptimal trajectories obtained via the approach

suggested in [5] are inferior to the optimal trajectories generated by the methods presented herein, from the viewpoint of estimation performance.

This work addresses the problem of optimizing observer trajectories in the context of discrete-time measurements. Motivated by [5], the approach taken in this work is based on directly maximizing the determinant of the FIM, which is used as a performance measure for the estimation process. However, unlike previous works, this work extends the problem formulation to address the issue of constraints on the observer trajectory. Such constraints might indeed arise in practice, e.g., due to threats to the observer, generated by the defense system which might be used by the target against the observer. Mathematical models are suggested, that account for both soft and hard constraints. Due to the complexity of the resulting performance index, the resulting optimal control problem is not amenable to classical control theory methods. Therefore, *direct* optimal control methods are used, which are based on parameterizing the control history using a fixed set of constant parameters, thus converting the infinite-dimensional optimal control problem into a finite-dimensional, static, parameter optimization one. Two direct, gradient-based numerical procedures are suggested herein. In addition, to facilitate the incorporation of hard state constraints, another procedure is used, based on the recently introduced differential inclusion (DI) approach [6]. The superiority of the optimal trajectories over arbitrarily generated trajectories and over suboptimal trajectories generated by Hammel's lower bound method [5] is demonstrated via a Monte Carlo analysis, using the Stansfield [1] and the ML [2] estimators.

In Section II, the problem of bearings-only optimal observer trajectories is mathematically formulated. Both unconstrained and constrained problem formulations are addressed. In Section III the numerical procedures utilized to solve the optimal control problem are presented. A simulation study, presented in Section IV, was carried out to demonstrate the enhancement to estimation performance using the optimal trajectories. This study used the Stansfield and ML estimators, which are presented in the Appendices for completeness. Concluding remarks are offered in Section V.

II. PROBLEM DEFINITION

The geometry of the bearings-only target localization problem is shown in Fig. 1 for the time instant t_k.

The observer position at this time is given by $\mathbf{x}_{S_k} = (x_{S_k}, y_{S_k})^T$. Using an onboard (commonly electro-optical) sensor, the observer measures the angle θ_k of its line of sight to the fixed target, which is located at $\mathbf{x}_T = (x_T, y_T)^T$. The objective of the

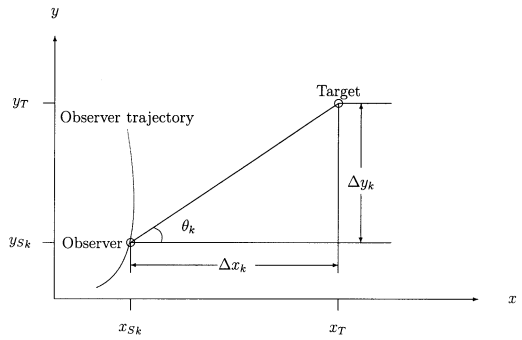

Fig. 1. Geometry of bearings-only localization problem.

observer is to estimate the target coordinates, based on a sequence of N measurements $\Theta = (\theta_1, \theta_2, \ldots, \theta_N)^T$, taken over the time interval $[0, T]$.

Assuming that the observer is moving at a constant speed V, its kinematic equations of motion are

$$\dot{x}_S(t) = V \cos u(t), \qquad x_S(0) = x_{S_0} \tag{1a}$$

$$\dot{y}_S(t) = V \sin u(t), \qquad y_S(0) = y_{S_0} \tag{1b}$$

where $u(t)$ is the instantaneous observer course at time t, measured with respect to the x axis, and the raised dot indicates the temporal derivative.

The measurement equation is

$$\theta_k = \arctan\left(\frac{y_T - y_{S_k}}{x_T - x_{S_k}}\right) + v_k \tag{2}$$

where $\{v_k\}_{k=1}^N$ is a zero-mean, Gaussian white noise sequence with constant variance σ^2.

The problem now is to determine an optimal observer trajectory, such that a maximal measure of information is extracted from the data set Θ, subject to various constraints.

A suitable measure for the information contained in Θ can be derived using the FIM [7]. As is well known, the relation between the FIM and the estimation error covariance matrix is established by means of the Cramer–Rao lower bound (CRLB). According to the CRLB Theorem, for a nonrandom parameter $\mathbf{x}_0$ and an unbiased estimator of this parameter $\hat{\mathbf{x}}(\Theta)$, where Θ represents the set of measurements, the estimation error covariance matrix is bounded by the lower bound

$$\mathbf{P} = E\{(\hat{\mathbf{x}}(\Theta) - \mathbf{x}_0)(\hat{\mathbf{x}}(\Theta) - \mathbf{x}_0)^T\} \geq \mathbf{M}^{-1} \tag{3}$$

where $\mathbf{M}$ is the FIM given by

$$\mathbf{M} = -E\left\{\frac{\partial^2}{\partial \mathbf{x}^2} \log p_{\Theta|\mathbf{x}}(\Theta \mid \mathbf{x})\right\}_{\mathbf{x}=\mathbf{x}_0} \tag{4}$$

and $p_{\Theta|\mathbf{x}}(\Theta \mid \mathbf{x})$ is the conditional probability density function. Notice that equality in (3) corresponds to an *efficient* estimator.

Since the estimation error covariance matrix is positive semidefinite, its associated quadratic form defines a hyperellipsoid depicting the distribution of

errors. The sizes of the semiaxes of this hyperellipsoid are defined by the eigenvalues of $\mathbf{P}$, and the orientations of these semiaxes are defined by the eigenvectors of $\mathbf{P}$. The one-sigma area of the ellipse corresponding to the two-dimensional case can be expressed as

$$A_{1\sigma} = \pi\sqrt{\det \mathbf{P}}. \tag{5}$$

Thus, generating the most observable trajectory is based on the minimization of the area given by (5), computed using the estimation error covariance matrix. As indicated by (3), for an efficient estimator, the error covariance matrix and the FIM are inversely related. Hence, for an efficient estimator, the area of the one-sigma uncertainty region for the two-dimensional case can also be expressed as

$$A_{1\sigma} = \frac{\pi}{\sqrt{\det \mathrm{FIM}}}. \tag{6}$$

Based on the foregoing discussion, the approach taken in this work is based on maximizing the determinant of the FIM, which is used as a performance measure for the estimation process. Maximizing the determinant of the FIM can be achieved through observer maneuvers since it is a function of vehicle motion. The specific role of the observer in the overall estimation process is to create a favorable target/observer geometry, so as to maximize system observability, thereby minimizing the region of uncertainty to enhance estimation accuracy.

In the present problem, the FIM can be expressed as

$$\mathrm{FIM} = \begin{bmatrix} \sum_{k=1}^{N} \dfrac{(\Delta y_k)^2}{\sigma_k^2 r_k^4} & -\sum_{k=1}^{N} \dfrac{\Delta x_k \Delta y_k}{\sigma_k^2 r_k^4} \\ -\sum_{k=1}^{N} \dfrac{\Delta x_k \Delta y_k}{\sigma_k^2 r_k^4} & \sum_{k=1}^{N} \dfrac{(\Delta x_k)^2}{\sigma_k^2 r_k^4} \end{bmatrix} \tag{7}$$

where

$$\Delta x_k \triangleq x_T - x_{S_k} \tag{8a}$$

$$\Delta y_k \triangleq y_T - y_{S_k} \tag{8b}$$

$$r_k^2 \triangleq (\Delta x_k)^2 + (\Delta y_k)^2. \tag{8c}$$

In passing, it is noted that although, as shown previously, the determinant of FIM is directly related to the area of the uncertainty ellipse, other scalar measures, e.g., the trace of the FIM, or the maximal eigenvalue of this matrix, could also be utilized (since minimizing these measures would lead to an effective minimization of the determinant). Although such alternative measures were not employed in this study, it is believed that the differences between the alternative measures would be mainly in the numerical behavior of the resulting optimization algorithms.

The following three problem formulations are considered.

A. Unconstrained Localization

In the case that no active constraint on the observer trajectory exists, the problem of observer trajectory optimization is formulated as follows:

Maximize the performance index:

$$J = \det \mathrm{FIM} \tag{9}$$

subject to the equations of motion (1) and the observation equation (2).

B. Soft State Constraints

In reality, the target might be defended against hostile observers. In this work, the following mathematical model is used to model the target defense system. The total threat "cost" over the time interval $[0,T]$ is assumed to be represented by

$$J_{\mathrm{Threat}} = \int_0^T G[\mathbf{x}_S(t)]\,dt \tag{10}$$

where $G[\mathbf{x}]$ is a known spatial "threat intensity function." For example, let the target be defended by M point defense subsystems (e.g., anti-aircraft guns, air-to-ground missiles, etc.) whose locations, denoted by $\{\mathbf{x}_{d_i}\}_{i=1}^{M}$ (where $\mathbf{x}_{d_i} = (x_{d_i}, y_{d_i})^T$) are assumed to be known. Furthermore, assume that the "threat intensities" associated with these defense systems are quantified by $\{p_i\}_{i=1}^{M}$. Assuming that the threat to the observer, generated by each defense subsystem, is inversely proportional to the distance between the observer and the defense subsystem, we have

$$G[\mathbf{x}_S(t)] = \sum_{i=1}^{M} \frac{p_i}{\sqrt{(x_S(t) - x_{d_i})^2 + (y_S(t) - y_{d_i})^2}}. \tag{11}$$

It is noted that the particular numerical methods used in this work can handle other threat models as well.

Using the above threat model, the problem can now be formulated as follows.

Maximize the performance index:

$$J = \alpha \det \mathrm{FIM} + \kappa(\alpha - 1)\int_0^T G[\mathbf{x}_S(\tau)]\,d\tau \tag{12}$$

subject to the equations of motion (1) and the observation equation (2).

In (12), κ is a normalization constant which is chosen to balance the difference in order of the two parts in (12), and $\alpha \in (0,1]$ is a weighting constant, determined so as to properly weigh accurate target localization versus observer survivability.

C. Hard State Constraints

Another way to take into consideration the defense system which might be used by the target against the observer is to incorporate hard state constraints into the optimization problem. The optimization problem in this case can be formulated as follows.

Maximize the performance index:

$$J = \det \mathrm{FIM} \tag{13}$$

subject to the equations of motion (1), the observation equation (2), and the state inequality constraints

$$g_p(x_S(t), y_S(t)) \le 0 \qquad p = 1, \ldots, M \quad t \in [0, T] \tag{14}$$

where M is the number of constraints.

In passing, we note that the particular performance measures chosen in this section preclude using classical solution methods based on the minimum principle. Therefore, in the next section we present numerical optimization procedures, which are used to solve the optimal control problem.

III. NUMERICAL SOLUTION

In this section we present three direct numerical methods, that were used to generate solutions for the previously formulated optimal control problem.

A. Direct Gradient-Based Method

The first method presented is a direct gradient-based method. For the sake of presentation, consider the following general optimal control problem.

Let the system equations of motion be given by

$$\begin{aligned} \dot{\mathbf{x}}(t) &= f(\mathbf{x}(t), \mathbf{u}(t), t) \\ \mathbf{x}(0) &= \mathbf{x}_0 \end{aligned} \tag{15}$$

where $\mathbf{x} \in \mathbb{R}^n$ and $\mathbf{u} \in (C^1[0,T])^m$, where $(C^1[0,T])^m$ denotes the set of all smooth functions that map the interval $[0,T]$ into $\mathbb{R}^m$. The optimization objective is to find the optimal control function $\mathbf{u}(t)$, $t \in [0,T]$, which minimizes a given cost functional

$$J = J(\mathbf{x}, \mathbf{u}) \tag{16}$$

subject to the system equations of motion (15). Notice that the problem is not assumed to be a Bolza problem [8–10].

The following approach is adopted in order to solve the optimization problem. Instead of searching for the optimal control history $\mathbf{u}(t)$, $t \in [0,T]$, the continuous control history is replaced by a *discretized* version, whose nodal values are given at a set of time points $\{t_k\}_{k=0}^{N-1}$, and an interpolation. Let $\mathbf{U}$ denote the vector of discretized control history over the time interval $[0,T]$, i.e.,

$$\mathbf{U} \triangleq [\mathbf{u}^T(t_0), \mathbf{u}^T(t_1), \ldots, \mathbf{u}^T(t_{N-1})]^T \in \mathbb{R}^{Nm}. \tag{17}$$

Here $\mathbf{U} \in \mathcal{U}$, where $\mathcal{U}$ is the set of admissible controls. Note that this parameterization of the control vector essentially transforms the *dynamic* optimal control problem into a *static* parameter optimization problem, where the parameters are all the entries of the discretized control history vector $\mathbf{U}$.

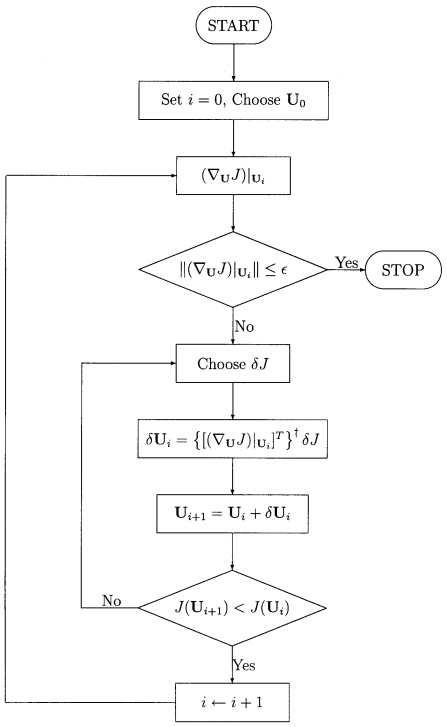

Fig. 2. Direct optimization procedure.

The solution procedure is outlined in Fig. 2. In this figure, the control history correction vector $\delta\mathbf{U}$ is computed by the algorithm developed next. Consider the first variation of the cost functional, which can be written as

$$\delta J = (\nabla_{\mathbf{U}} J)^T \delta \mathbf{U} \tag{18}$$

where $\nabla_{\mathbf{U}} J$ is the gradient of the cost functional with respect to the control history vector, and $\delta\mathbf{U}$ is the variation of the control history vector. The cost functional gradient can be computed numerically, using some numerical scheme (e.g., first-order forward difference).

Let the first variation of the cost functional δJ be arbitrarily chosen such that $\delta J < 0$. Then, the implied required control variation can be obtained, in principle, by solving the following set of linear equations

$$A \delta \mathbf{U} = \delta J \tag{19}$$

where

$$A \triangleq (\nabla_{\mathbf{U}} J)^T. \tag{20}$$

However, since (20) constitutes an *underdetermined* system of equations, it possesses an infinite number of solutions. Therefore, the unique minimum-norm least squares solution is chosen, which is defined by

$$\delta\mathbf{U}_{\mathrm{LS}} \triangleq \arg\min_{\delta\mathbf{U}\in\mathcal{X}} \|\delta\mathbf{U}\|_2 \tag{21}$$

where

$$\mathcal{X} \triangleq \{\delta\mathbf{U}\in\mathcal{U} \mid \|A\delta\mathbf{U}-\delta J\|_2 \to \min\}. \tag{22}$$

To compute $\delta\mathbf{U}_{\mathrm{LS}}$, the Moore–Penrose generalized inverse of A is used:

$$\delta\mathbf{U}_{\mathrm{LS}} = A^{\dagger}\,\delta J. \tag{23}$$

REMARK 1 A numerically stable algorithm for computing $A^{\dagger}$ is based on the singular value decomposition (SVD) of A [11].

REMARK 2 Like in every gradient-based method, the initial guess might affect the convergence of the solution process, if the cost function is neither convex nor concave. Hence, physical insight should be utilized in properly choosing the initial guess.

REMARK 3 The computation of the cost functional $J(\mathbf{U}_i)$ involves a complete solution of the differential equations of motion for the interpolated control history vector. Therefore, the computational burden associated with the resulting numerical scheme is relatively high.

B. Orthogonal Function Parameterization

The obvious problem of the direct method presented in the previous subsection is the large number of optimization parameters, which are the elements of the control history vector $\mathbf{U}$. To alleviate this problem, we take the following approach.

Instead of directly discretizing the control history, we can parameterize the control vector using the following series:

$$\mathbf{u}(t) = \sum_{i=1}^{p} a_i\phi_i(t) \tag{24}$$

where the functions $\{\phi_i(t)\}_{i=1}^{p}$ are taken from a complete set of orthogonal basis functions. In this work, two such sets were utilized: the Chebychev and Laguerre polynomial series [12]. Chebychev polynomials are generated using the following recurrence:

$$\begin{aligned} &T_0(x) = 1, \qquad T_1(x) = x \\ &T_{n+1}(x) = 2xT_n(x) - T_{n-1}(x), \qquad n = 1,2,\ldots . \end{aligned} \tag{25}$$

Laguerre polynomials are generated using the recurrence

$$\begin{aligned} &L_0(x) = 1, \qquad L_1(x) = 1-x \\ &L_{n+1}(x) = (2n+1-x)L_n(x) - n^2L_{n-1}(x), \qquad n = 1,2,\ldots . \end{aligned} \tag{26}$$

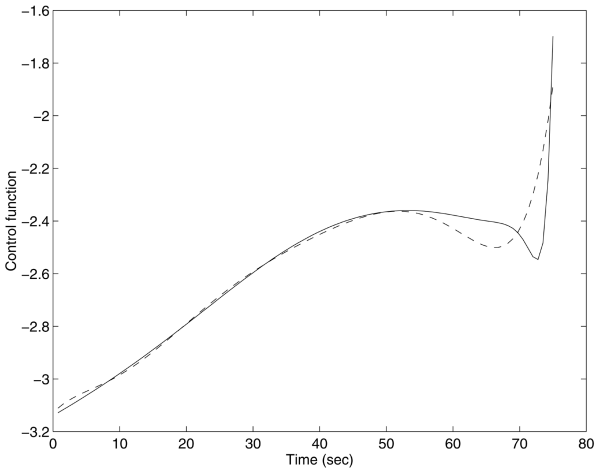

Fig. 3. Optimal control function using a) direct control discretization, 100 sampling points (solid), and b) orthogonal (Chebychev) polynomial series approximation, 8 terms (dashed).

Using now (24) in the equations of motion (15) yields a new parameterization of the optimization problem in terms of the parameter vector $\mathbf{a} \triangleq \mathrm{col}(a_1,a_2,\ldots,a_p)$, namely

$$\min_{\mathbf{a}} J(\mathbf{x}(t),\mathbf{a}) \tag{27}$$

subject to the following system equations of motion

$$\begin{aligned} \dot{\mathbf{x}}(t) &= f(\mathbf{x}(t),\mathbf{a},t) \\ \mathbf{x}(0) &= \mathbf{x}_0 \end{aligned} \tag{28}$$

where $\mathbf{x}\in\mathbb{R}^n$ and $\mathbf{a}\in\mathbb{R}^p$. To solve this problem, the method presented previously can be utilized.

To demonstrate the performance of this method, we compared it with the direct discretization method using a typical example. In this example, the target is located in the origin, the observer trajectory starts at $\mathbf{x}_{S_0} = (5000,0)^T$ m, the bearing measurement noise standard deviation is 3 mrad and the observer velocity is 40 m/s. 100 measurements are acquired uniformly over an observation interval of 75 s. Fig. 3 depicts the control functions as computed using: a) the direct control discretization method of the previous section, using 100 sampling points of the control function $\mathbf{u}(t)$, and b) the orthogonal polynomial parameterization method, (24), using 8 Chebychev polynomials (i.e., $p = 8$). In both cases, the optimization procedure started from an initial control function obtained using Hammel's lower bound method (see Section IV). As can be seen from Fig. 3, the difference between the two control functions is relatively small. In fact, the resulting difference in the value of the performance index is 0.1%. However, the saving in computation time is very substantial, since, using the orthogonal polynomial method, the optimization was carried out over an 8-dimensional parameter space, as opposed to a 100-dimensional parameter space in the direct discretization method. In passing, it is noted that similar results were obtained using the Laguerre series with the same number of terms.

C. Differential Inclusion Solution

A common problem with direct methods is that there is no clear and simple way to incorporate state and control constraints into the solution. The recently introduced differential inclusion (DI) method [6] handles these constraints easily, by employing a description of the dynamical system in terms of its states and their sets of attainability, in favor of using differential equations, thus completely eliminating the controls from the system mathematical model. In this section we use this technique to introduce a method for generating finite-dimensional approximations to the solution of the constrained optimal localization problem.

For conciseness, the fundamental theory of the DI method itself is not discussed here. The interested reader is referred to [6] for an excellent presentation of the method. Rather, in this section we concentrate on the application of the DI method to our problem.

Notice that in the problem under consideration the control can be eliminated using the equations of motion (1), as follows

$$(\dot{x}_S)^2 + (\dot{y}_S)^2 = V^2. \tag{29}$$

Equation (29) represents the *hodograph* of the system, which is defined as the set of all possible state rates that can be achieved by varying the controls within their allowed bounds. Hence, the formulation of our optimization problem in terms of the DI approach proceeds as follows.

Let n be a chosen integer, and define $n+1$ equidistant nodes

$$t_i = \frac{i}{n}T, \qquad i = 0,1,\ldots,n. \tag{30}$$

The values of the states $(x_{S_i}, y_{S_i})^T$ at the nodes $\{t_i\}_{i=0}^n$ are obtained from solving the following nonlinear programming problem

$$\max_{\{x_{S_i}, y_{S_i}\}_{i=0}^n} \det \mathrm{FIM} \tag{31}$$

subject to the initial conditions

$$x_{S_0} = x_S(0), \qquad y_{S_0} = y_S(0) \tag{32}$$

and

$$(\dot{\overline{x}}_i)^2 + (\dot{\overline{y}}_i)^2 = V^2 \qquad i = 0,1,\ldots,n-1 \tag{33}$$

where

$$\dot{\overline{x}}_i \triangleq \frac{x_{S_{i+1}} - x_{S_i}}{\Delta t}, \qquad \dot{\overline{y}}_i \triangleq \frac{y_{S_{i+1}} - y_{S_i}}{\Delta t} \tag{34}$$

and detFIM is computed via (7) in terms of the optimization variables.

Additional state inequality constraints can be directly imposed for specific problem formulations, as

$$g_l(\{x_{S_i}\}_{i=0}^{n-1}, \{y_{S_i}\}_{i=0}^{n-1}) \le 0, \qquad l = 1,\ldots,q. \tag{35}$$

For example, if the constraint is a circle of radius R_c centered at the origin, the state inequality constraint is incorporated by solving the nonlinear programming problem subject to the additional constraints

$$(x_{S_i})^2 + (y_{S_i})^2 \ge (R_c)^2, \qquad i = 0,1,\ldots,n. \tag{36}$$

In passing, it should be noted that although in our case the control functions are assumed to be smooth, the DI approach is not limited to smooth control functions and can handle piecewise continuous control functions as well [6].

IV. SIMULATION STUDY

An extensive numerical simulation study was performed, in order to assess and demonstrate the characteristics of the new approach. Several target localization scenarios were considered, both with and without the presence of threat to the observer. In all examples in the sequel, the observer trajectory starts at $\mathbf{x}_{S_0} = (5000,0)^T$ m, the bearing measurement noise is assumed zero-mean, Gaussian distributed with $\sigma = 3$ mrad, and the observer velocity is $V = 40$ m/s. The target is located at the origin, i.e., $\mathbf{x}_T = (0,0)^T$ m. Except where otherwise noted, 100 measurements were uniformly acquired over the observation trajectory.

A. Comparison With Lower-Bound Method

The purpose of this example is to compare the performance of the new approach with Hammel's detFIM lower bound method [5]. No threat to the observer was considered in this example.

Let K be the nondimensional parameter

$$K \triangleq \frac{VT}{R_0} \tag{37}$$

where R_0 is the observer's initial range to the target. Obviously, $0 < K < 1$. Notice that K represents the observer's ability (for given initial range, observation time and speed) to approach the target (thus, if the observer trajectory consists of a straight line, then $K = 1$ represents the trivial case where the observer can hit the target at the end of its trajectory).

Fig. 4 shows several optimal trajectories, corresponding to varying values of K. As can be expected, as K becomes larger, the observer trajectories end nearer to the target. Notice also the interesting trade-off, exhibited by the trajectories, between the need to approach the target (see (7)) and the need to increase the bearing-rate (this trade-off was observed also in [5]). For scenarios with small effective baseline-to-range ratios, maximizing bearing-rate is of primary importance. For scenarios

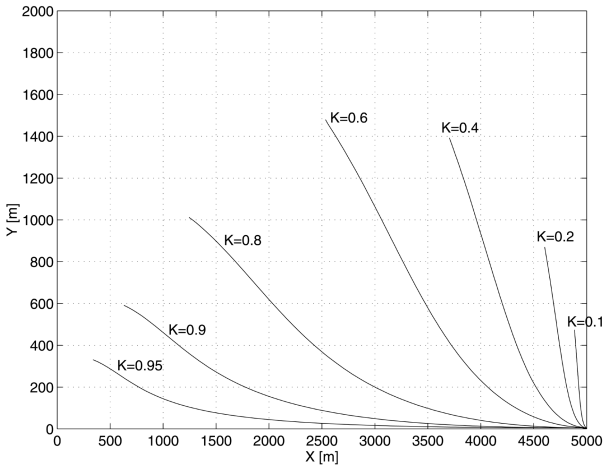

Fig. 4. Optimal trajectories for various values of parameter K.

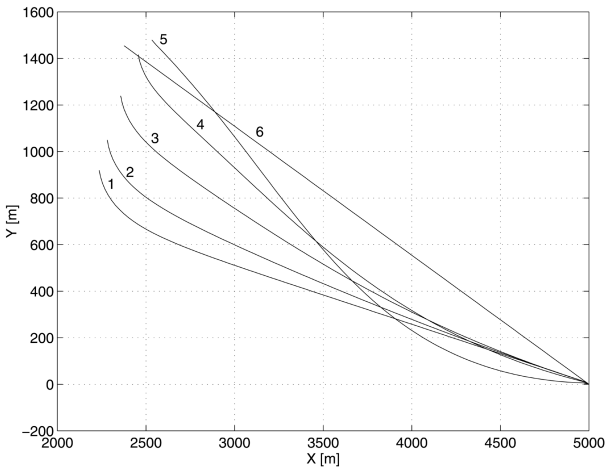

Fig. 5. Observer trajectories.

with large ratios, on the other hand, the optimal trajectories primarily aim at reducing the range to the target. Notice that the importance of maximizing the bearing-rate for obtaining maximal observability in the bearings-only localization problem is discussed in great detail in [4].

As previously mentioned, Hammel, et al. [5] proposed to replace the detFIM performance index by a *lower bound* on detFIM, which may be computed as [5]

$$J' = \frac{1}{\sigma^2}\int_0^T \frac{\dot{\theta}}{r^2}\,d\tau \tag{38}$$

where θ is the (measured) bearing angle and r is the observer's range to the target.

Fig. 5 shows six observer trajectories, computed for $K = 0.6$ and $\alpha = 1$. Trajectory 1 in this figure is the result of optimization with respect to Hammel's lower bound performance index, (38). Trajectory 5 is optimal with respect to the detFIM performance index, (12). This trajectory resulted from using the iterative optimization process shown in Fig. 2, starting from trajectory 1 as an initial guess. Trajectories 2–4 are nonoptimal trajectories, obtained as intermediate results during the iterative optimization process, and trajectory 6 is the optimal *straight line* trajectory, i.e., the best (in terms of detFIM) of all straight line trajectories.

Table I compares the value of detFIM as a function of K, for three types of trajectories: 1) trajectories generated via directly maximizing detFIM, 2) trajectories generated via maximizing Hammel's lower bound, and 3) optimal straight line trajectories. As can be observed from the table, trajectories resulting from directly maximizing detFIM are clearly superior to other trajectories.

TABLE I
Det FIM for Various Optimal Trajectories

Performance Index	$K = 0.1$	$K = 0.2$	$K = 0.4$	$K = 0.6$
det FIM	1.7202E-04	7.6456E-04	0.0044	0.0190
Lower Bound	1.6470E-04	7.3924E-04	0.0041	0.0113
Constrained det FIM*	1.6891E-04	7.3105E-04	0.0041	0.0174

Note: *Optimal straight line.

B. Differential Inclusion Example

To demonstrate the performance of the DI method, the trajectory optimization problem was solved under the additional hard state constraint

$$\|\mathbf{x}_S(t) - \mathbf{x}_T\| \geq R \qquad \forall \quad t \tag{39}$$

where $R = 4000$ m. In this example 20 measurements were acquired, the value of K was set to 0.6 and no threat to the observer was considered. For the numerical solution of the nonlinear programming problem, the gradient-based CONSTR routine of the MATLAB optimization toolbox [13] was utilized. This routine is based on sequentially solving quadratic programming sub-problems.

Fig. 6 shows the optimal trajectories obtained with and without the constraint. As can be expected from the shape of the unconstrained optimal trajectory, when the constraint is active, the trajectory ends on the constraint (a circle centered at the origin with a radius of 4000 m).

C. Effect of Threat

In this example, a threat intensity function was assumed according to

$$G[\mathbf{x}_S(t)] = \max\left\{\sum_{i=1}^{5}\frac{p_i}{\sqrt{(x_S(t)-x_{d_i})^2 + (y_S(t)-y_{d_i})^2}}, 1\right\}. \tag{40}$$

The parameters of $G[\mathbf{x}_S(t)]$ are listed in Table II. A three-dimensional plot of the function $G[\mathbf{x}_S(t)]$ in the first quadrant of the X-Y plane is shown in Fig. 7. The performance index used was as in (12) with $\kappa = 0.01$, and the value of K was set to 0.8.

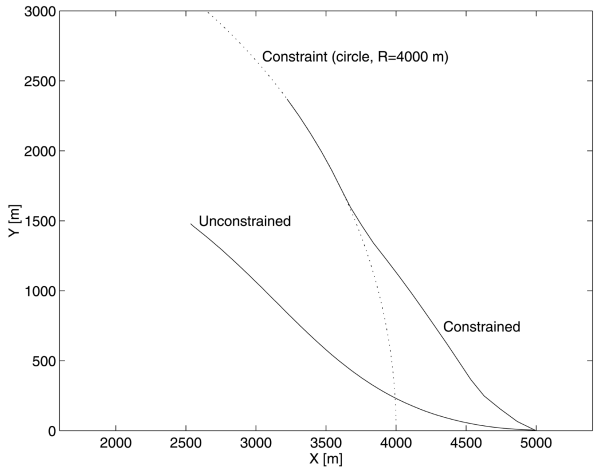

Fig. 6. DI example. Dotted line represents constraint.

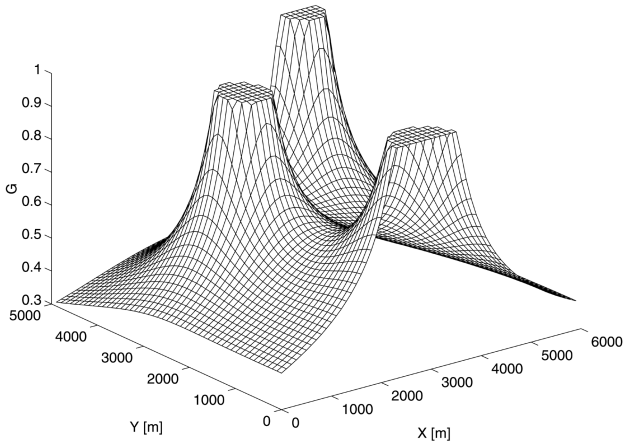

Fig. 7. Threat function in first quadrant of X-Y plane. Target is located at origin.

TABLE II
Parameters of $G[\mathbf{x}]$

i	p_i	x_{d_i}	y_{d_i}
1	300	3000	0
2	200	2000	3000
3	200	2000	−3000
4	200	4949	4949
5	200	4949	−4949

Fig. 8 shows different observer trajectories, superimposed on lines of constant threat intensity. The observer trajectories were generated for varying threat weighting factors, listed in Table III (note that $\alpha = 1$ corresponds to a "no-threat" scenario).

As can be observed from the figure, as the threat weighting factor increases, the observer trajectory deviates to increase observer's survivability. This, however, decreases the attainable estimation performance, as can be observed from Table III, which shows values of detFIM computed for the six trajectories.

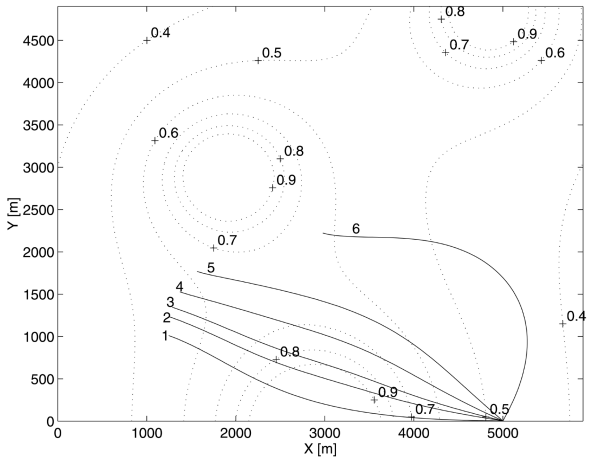

Fig. 8. Optimal trajectories in presence of threat.

TABLE III
DetFIM Versus Threat Intensity

Trajectory	α	detFim
1	1	0.1160
2	0.8	0.1068
3	0.7	0.0967
4	0.6	0.0730
5	0.5	0.0483
6	0.4	0.0081

D. Actual Localization Performance

To verify the actual performance of common estimators along optimal trajectories generated by both the new method and Hammel's lower bound method, the Stansfield and ML estimators were utilized in a Monte-Carlo simulation study (for completeness, these estimators are reviewed in the Appendices).

The Monte-Carlo study consisted of $M = 1000$ computer runs. No threat to the observer was considered, and a value of $K = 0.6$ was used in all runs. The six trajectories shown in Fig. 5 were tested. The estimation error in each run was computed as $\tilde{\mathbf{x}}_T = (\tilde{x}_T, \tilde{y}_T)$. The average estimation errors $\overline{x}_T \stackrel{\Delta}{=} 1/M \sum_{i=1}^{M} \tilde{x}_{T_i}$ and $\overline{y}_T \stackrel{\Delta}{=} 1/M \sum_{i=1}^{M} \tilde{y}_{T_i}$ as well as the estimation error standard deviations σ_{x_T} and σ_{y_T} were computed. The Monte Carlo study results are presented in Table IV. As can be observed from the table, the optimal trajectory computed using (12), which exhibits the largest detFIM value, is associated with the best estimation performance, for both estimators. Notice also that, as could be expected, the ML estimator, which is asymptotically unbiased, is clearly superior to the Stansfield estimator.

V. CONCLUSIONS

This paper has presented methods to compute optimal observer trajectories for bearings-only localization of a stationary target. The role of these trajectories is to create a target/observer geometry that

TABLE IV
Actual Performance of ML and Stansfield Estimators

Trajectory	det FIM	ML Estimator				Stansfield Estimator			
		$\bar{x}_T$	$\bar{y}_T$	σ_{x_T}	σ_{y_T}	$\bar{x}_T$	$\bar{y}_T$	σ_{x_T}	σ_{y_T}
1[a]	0.0113	−0.102	−0.024	8.888	1.864	−2.396	−0.330	11.918	1.842
2[b]	0.0136	−0.004	−0.034	7.828	1.875	−1.485	−0.293	10.257	1.835
3[b]	0.0165	−0.478	−0.118	6.712	1.828	−1.785	−0.373	8.650	1.775
4[b]	0.0183	−0.161	−0.041	6.219	1.839	−1.089	−0.185	7.601	1.777
5[c]	0.0190	−0.001	−0.004	6.203	1.819	−0.867	−0.175	7.503	1.728
6[d]	0.0174	0.035	0.008	6.477	2.173	−1.049	−0.243	8.047	2.104

Note: [a]Optimal in sense of Hammel's lower bound (eq. (38)). [b]Nonoptimal. [c]Optimal in sense of det FIM (eq. (12)). [d]Optimal straight line.

maximizes system observability, thereby enhancing estimation accuracy. The approach presented in this work is based on directly maximizing the determinant of the FIM, while taking into account (soft and hard) constraints imposed on the observer trajectory by the target defense system.

Since the resulting performance index is not amenable to classical control theory methods based on the minimum principle, direct methods were used. These include two gradient-based numerical procedures and a method based on the recently introduced DI technique. Using these methods, the dynamic optimal control problem is effectively transformed into a static parameter optimization one, which can then be solved using any nonlinear programming procedure.

To verify the actual performance of bearings-only estimators along optimal trajectories, the widely used Stansfield and ML estimators were utilized in an extensive Monte Carlo simulation study. The study demonstrated the enhancement to target position estimability using the optimal observer trajectories.

Finally, although this paper was concerned with the static, 2-dimensional target localization problem, the approach presented here can be readily extended to the 3-dimensional case. The treatment of maneuvering targets (i.e., bearings-only tracking), as well as the inclusion of prior information on the target position via probabilistic models, should provide interesting topics for further research.

APPENDIX A. STANSFIELD ESTIMATOR

For the sake of completeness, we review herein the Stansfield estimator (also called pseudo-linear estimator) [1], which is used in our numerical study. Whereas Stansfield considered the particular case where the bearing measurements are corrupted by random zero mean noise, and the observer trajectory is assumed to be perfectly known, Ancker [14] extended the Stansfield solution to include the case of observer navigation errors, which introduce uncertainties in the passive sensor location. Blachman [15] presented a new, simpler derivation for the Stansfield estimator, making an underlying assumption that the observation points are regularly spaced along a simple curve or straight line.

The Stansfield estimator is defined by

$$\hat{\mathbf{x}}_{T\mathrm{ST}} \triangleq \arg\min_{\mathbf{x}_T} F_{\mathrm{ST}}(\mathbf{x}_T, \Theta) \tag{41}$$

where

$$F_{\mathrm{ST}}(\mathbf{x}_T, \Theta) = \frac{1}{2}\sum_{k=1}^{N} \frac{\sin^2 \Delta\theta_k}{\sigma_k^2}. \tag{42}$$

Carrying out the minimization of the cost functional in (42) yields

$$\hat{\mathbf{x}}_{T\mathrm{ST}} = (\mathbf{A}^T\mathbf{R}^{-1}\mathbf{W}\mathbf{A})^{-1}\mathbf{A}^T\mathbf{R}^{-1}\mathbf{W}\mathbf{b} \tag{43}$$

where we have defined

$$\mathbf{A} \triangleq \begin{bmatrix} \sin\theta_1 & -\cos\theta_1 \\ \vdots & \vdots \\ \sin\theta_N & -\cos\theta_N \end{bmatrix} \tag{44}$$

$$\mathbf{b} \triangleq \begin{bmatrix} x_{S_1}\sin\theta_1 - y_{S_1}\cos\theta_1 \\ \vdots \\ x_{S_N}\sin\theta_N - y_{S_N}\cos\theta_N \end{bmatrix} \tag{45}$$

$$\mathbf{R} \triangleq \mathrm{diag}\{r_1^2, \ldots, r_N^2\} \tag{46}$$

$$\mathbf{W} \triangleq \mathrm{diag}\{\sigma_1^2, \sigma_2^2, \ldots, \sigma_N^2\} \tag{47}$$

and r_k^2 is defined in (8c).

Note that in (43) the matrix $\mathbf{R}$ is assumed known. In practice, this is not true since $\mathbf{R}$ depends on the relative position of the observer with respect to the target, however, this matrix can be approximated since the cost function (42) depends only weakly on $\mathbf{R}$.

APPENDIX B. MAXIMUM LIKELIHOOD ESTIMATOR

To develop the ML estimator [2], rewrite the measurement equation as

$$\theta_k = g(\mathbf{x}_T, \mathbf{x}_{S_k}) + v_k, \qquad k = 1, \ldots, N \tag{48}$$

where the nonlinear observation function is

$$g(\mathbf{x}_T, \mathbf{x}_{S_k}) \triangleq \arctan\left(\frac{y_T - y_{S_k}}{x_T - x_{S_k}}\right). \tag{49}$$

Let $\hat{\mathbf{x}}_S$ denote the set of observer positions at which measurements were acquired, i.e.,

$$\hat{\mathbf{x}}_S \triangleq [\mathbf{x}_{S_1} \quad \mathbf{x}_{S_2} \quad \cdots \quad \mathbf{x}_{S_N}]^T. \tag{50}$$

Defining the vector of nonlinear observation functions as

$$\mathbf{g}(\mathbf{x}_T, \hat{\mathbf{x}}_S) \triangleq [g(\mathbf{x}_T, \mathbf{x}_{S_1}) \quad g(\mathbf{x}_T, \mathbf{x}_{S_2}) \quad \cdots \quad g(\mathbf{x}_T, \mathbf{x}_{S_N})]^T \tag{51}$$

and the observation noise vector as

$$\mathbf{v} = [v_1 \quad v_2 \quad \cdots \quad v_N]^T \tag{52}$$

yields

$$\Theta = \mathbf{g}(\mathbf{x}_T, \hat{\mathbf{x}}_S) + \mathbf{v} \tag{53}$$

where $\mathbf{v}$ is a zero-mean measurement noise vector, with covariance matrix $\mathbf{W}$. In terms of the above model, the joint conditional probability density function of the measurements given the target location $\mathbf{x}_T$ is

$$p(\Theta \mid \mathbf{x}_T) = \frac{1}{(2\pi)^{N/2}(\det \mathbf{W})^{1/2}} \times \exp\{-\tfrac{1}{2}[\Theta - \mathbf{g}(\mathbf{x}_T, \hat{\mathbf{x}}_S)]^T \mathbf{W}^{-1} [\Theta - \mathbf{g}(\mathbf{x}_T, \hat{\mathbf{x}}_S)]\}. \tag{54}$$

The ML estimator maximizes the log-likelihood function. Equivalently, it can be defined as

$$\hat{\mathbf{x}}_{T\mathrm{ML}} = \arg\min_{\mathbf{x}_T} F_{\mathrm{ML}}(\mathbf{x}_T, \Theta) \tag{55}$$

where the negative log-likelihood function is

$$F_{\mathrm{ML}}(\mathbf{x}_T, \Theta) = \tfrac{1}{2}(\Delta\Theta)^T \mathbf{W} (\Delta\Theta). \tag{56}$$

In (56), $\Delta\Theta$ is defined as

$$\Delta\Theta \triangleq \mathbf{g}(\mathbf{x}_T, \hat{\mathbf{x}}_S) - \Theta = (\Delta\theta_1, \ldots, \Delta\theta_N)^T \tag{57}$$

where

$$\Delta\theta_k(\mathbf{x}_T) = g(\mathbf{x}_T, \mathbf{x}_{S_k}) - \theta_k. \tag{58}$$

Using the above definitions, the negative log-likelihood function can be written as

$$F_{\mathrm{ML}}(\mathbf{x}_T, \Theta) = \frac{1}{2} \sum_{k=1}^{N} \frac{(\Delta\theta_k)^2}{\sigma_k^2}. \tag{59}$$

Equation (59) calls for a nonlinear minimization procedure, e.g., the Newton–Gauss method, i.e.,

$$\mathbf{x}_T^{i+1} = \mathbf{x}_T^i + \Delta\mathbf{x}_T^i, \qquad i = 0, \ldots, 1 \tag{60}$$

where

$$\Delta\mathbf{x}_T^i = \{[\nabla_{\mathbf{x}_T} \mathbf{g}^T(\mathbf{x}_T^i)]^T \mathbf{W}^{-1} \nabla_{\mathbf{x}_T} \mathbf{g}^T(\mathbf{x}_T^i)\}^{-1} \times [\nabla_{\mathbf{x}_T} \mathbf{g}^T(\mathbf{x}_T^i)]^T \mathbf{W}^{-1} \Delta\Theta(\mathbf{x}_T^i) \tag{61}$$

and $\nabla_{\mathbf{x}_T} \mathbf{g}^T(\mathbf{x}_T^i)$ is the gradient matrix of $\mathbf{g}^T$ with respect to $\mathbf{x}_T$, evaluated at $\mathbf{x}_T^i$. The Newton–Gauss iteration starts with a user-supplied initial condition $\mathbf{x}_T^0$, which is required to be close enough to the minimum, for rapid convergence.

The statistical efficiency of the method can be assessed by the covariance matrix of the estimation error $\tilde{\mathbf{x}}_{T\mathrm{ML}}$, which is computed by

$$\mathrm{cov}(\tilde{\mathbf{x}}_{T\mathrm{ML}}) = [\nabla_{\mathbf{x}_T} \mathbf{g}^T(\hat{\mathbf{x}}_{T\mathrm{ML}})]^T \mathbf{W}^{-1} \nabla_{\mathbf{x}_T} \mathbf{g}^T(\hat{\mathbf{x}}_{T\mathrm{ML}}). \tag{62}$$

Comparing the two estimators, it is clear that the Stansfield estimator requires less computations and, hence, is superior for real-time applications. However, as shown in [16], the Stansfield method leads to a biased estimator, even for a large number of measurements, while the ML estimator is asymptotically unbiased.

REFERENCES

[1] Stansfield, R. G. (1947)
Statistical theory of DF fixing.
Journal of the IEE, **14**, 15 (1947), 762–770.

[2] Nardone, S. C., Lindgren, A. G., and Gong, K. F. (1984)
Fundamental properties and performance of conventional bearings-only target motion analysis.
IEEE Transactions on Automatic Control, **AC-29** (Sept. 1984), 775–787.

[3] Aidala, V. J. (1979)
Kalman filter behavior in bearings-only tracking applications.
IEEE Transactions on Aerospace and Electronic Systems, **AES-15**, 1 (Jan. 1979), 29–39.

[4] Fawcett, J. A. (1988)
Effect of course maneuvers on bearings-only range estimation.
IEEE Transactions on Acoustics, Speech and Signal Processing, **36**, 8 (Aug. 1988), 1193–1199.

[5] Hammel, S. E., Liu, P. T., Hilliard, E. J., and Gong, K. F. (1989)
Optimal observer motion for localization with bearing measurements.
Computers and Mathematics with Applications, **18**, 1–3 (1989), 171–180.

[6] Seywald, H. (1994)
Trajectory optimization based on differential inclusion.
Journal of Guidance, Control, and Dynamics, **17**, 3 (May–June 1994), 480–487.

[7] Kay, S. M. (1993)
Fundamentals of Statistical Signal Processing: Estimation Theory.
Englewood Cliffs, NJ: Prentice-Hall, 1993.

[8] Ewing, G. M. (1969)
Calculus of Variations with Applications.
New York: Norton, 1969.

[9] Miele, A. (1962)
The calculus of variations in applied aerodynamics and flight mechanics.
In G. Leitmann (Ed.), *Optimization Techniques With Applications to Aerospace Systems*.
New York: Academic Press, 1962.

[10] Bryson, A. E., Jr., and Ho, Y.-C. (1975)
Applied Optimal Control—Optimization, Estimation and Control.
Taylor and Francis, 1975.

[11] Golub, G. H., and Van Loan, C. F. (1983)
Matrix Computations.
Baltimore, MD: The Johns Hopkins University Press, 1983.

[12] Ralston, A. (1965)
A First Course in Numerical Analysis.
New York: McGraw-Hill, 1965.

[13] Grace, A. (1993)
MATLAB Optimization Toolbox User's Guide.
The MathWorks, Inc., Natick, MA, June 1993.

[14] Ancker, C. J. (1958)
Airborne direction finding—The theory of navigation errors.
IRE Transactions on Aeronautical Navigation Electronics, **ANE-5** (Dec. 1958), 199.

[15] Blachman, N. M. (1969)
Position determination from radio bearings.
IEEE Transactions on Aerospace and Electronic Systems, **AES-5**, 3 (May 1969), 558–560.

[16] Gavish, M., and Weiss, A. J. (1992)
Performance analysis of bearing-only target location algorithms.
IEEE Transactions on Aerospace and Electronic Systems, **28**, 3 (July 1992), 817–828.

Yaakov Oshman (SM'97) received the B.Sc. (summa cum laude) and the D.Sc. degrees, both in aeronautical engineering, from the Technion–Israel Institute of Technology, Haifa, Israel, in 1975 and 1986, respectively.

From 1975 to 1981 he was with the Israeli Air Force, where he worked in the areas of structural dynamics and flutter analysis and flight testing. In 1987 he was a Research Associate at the Department of Mechanical and Aerospace Engineering at the State University of New York at Buffalo, where he was, in 1988, a Visiting Professor. Since 1989 he has been with the Department of Aerospace Engineering at the Technion–Israel Institute of Technology where he is currently an Associate Professor. During the 1996/1997 and 1997/1998 academic years he spent a sabbatical with the Guidance, Navigation and Control Center of NASA's Goddard Space Flight Center, where he worked in research and development of spacecraft attitude estimation algorithms. His reseach interests are in advanced optimal estimation and control methods and their application in aerospace systems.

Dr. Oshman is an Associate Fellow of the AIAA.

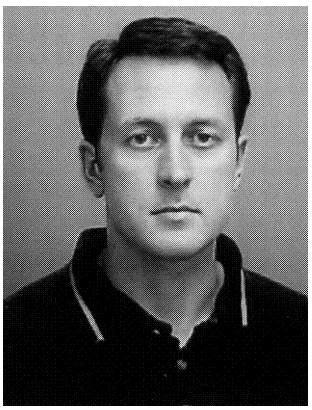

Pavel Davidson was born in Russia on March 16, 1968. He received his Diploma in aerospace engineering from the Moscow Institute of Physics and Technology in 1991. He received his M.Sc. in aerospace engineering in 1996 from the Technion–Israel Institute of Technology.

From 1988 to 1991 he was a research assistant at the Central Aerohydrodynamic Institute, Moscow, Russia, in the field of flight control and dynamics. From 1991 to 1992 he served as a research engineer at St. Petersburg Institute of Information and Automation. He joined Israel Aircraft Industries in 1996 and has been working there ever since.